

# Parapharyngeal Space: Diagnostic Imaging and Intervention

## Parapharyngealraum: bildgebende Diagnostik und Intervention

### Authors

Thomas J. Vogl<sup>1</sup> , Iris Burck<sup>1</sup>, Timo Stöver<sup>2</sup>, Rania Helal<sup>1,3</sup>

### Affiliations

- 1 Clinic for Radiology and Nuclear Medicine, Hospital of the Goethe University Frankfurt Center of Radiology, Frankfurt am Main, Germany
- 2 Clinic for Ear, Nose and Throat Medicine, Hospital of the Goethe University Frankfurt, Frankfurt am Main, Germany
- 3 Department of Diagnostic and Interventional Radiology, Ain Shams University Faculty of Medicine, Cairo, Egypt

### Keywords

pharynx, interventional procedures, head/neck, MR-imaging, MR-angiography

received 27.2.2024

accepted after revision 13.9.2024

published online 2024

### Bibliography

Fortschr Röntgenstr

DOI 10.1055/a-2419-9782

ISSN 1438-9029


© 2024, Thieme. All rights reserved.

Georg Thieme Verlag KG, Oswald-Hesse-Straße 50, 70469 Stuttgart, Germany

### Correspondence

Prof. Thomas J. Vogl

Clinic for Radiology and Nuclear Medicine, Hospital of the Goethe University Frankfurt Center of Radiology, Frankfurt am Main, Germany  
T.vogl@em.uni-frankfurt.de

 Deutsche Version unter: <https://doi.org/10.1055/a-2419-9782>.

### ABSTRACT

**Background** Diagnosis of lesions of the parapharyngeal space (PPS) often poses a diagnostic and therapeutic challenge due to its deep location. As a result of the topographical relationship to nearby neck spaces, a very precise differential diagnosis is possible based on imaging criteria. When in doubt, imaging-guided – usually CT-guided – biopsy and even drainage remain options.

**Method** Through a precise analysis of the literature including the most recent publications, this review precisely describes the basic and most recent imaging applications for various PPS pathologies and the differential diagnostic scheme for as-

signing the respective lesions in addition to the possibilities of using interventional radiology.

**Results** The different pathologies of PPS from congenital malformations and inflammation to tumors are discussed according to frequency. Characteristic criteria and, more recently, the use of advanced imaging procedures and the introduction of artificial intelligence (AI) allow a very precise differential diagnosis and support further diagnosis and therapy. After precise access planning, almost all pathologies of the PPS can be biopsied or, if necessary, drained using CT-assisted procedures.

**Conclusion** Radiological procedures play an important role in the diagnosis and treatment planning of PPS pathologies.

### Key Points

- Lesions of the PPS account for about 1–2% of all pathologies of the head and neck region. The majority are benign lesions and inflammatory processes.
- If differential diagnostic questions remain unanswered, material can – if necessary – be obtained via a CT-guided biopsy. Exclusion criteria are hypervascularized processes, especially paragangliomas and angiomas.
- The use of artificial intelligence (AI) in head and neck imaging of various pathologies, such as tumor segmentation, pathological TMN classification, detection of lymph node metastases, and extranodal extension, has significantly increased in recent years.

### Citation Format

- Vogl TJ, Burck I, Stöver T et al. Parapharyngeal Space: Diagnostic Imaging and Intervention. Fortschr Röntgenstr 2024; DOI 10.1055/a-2419-9782

### ZUSAMMENFASSUNG

**Hintergrund** Die bildgebende Diagnostik des Parapharyngealraums (PPR) stellt aufgrund der komplexen Lagebeziehung eine besondere Herausforderung an die bildgebende radiologische Diagnostik und Intervention dar. Dabei ist eine sehr gute und präzise Differenzialdiagnose anhand der Bildgebungskriterien und der topografischen Zusammenhänge möglich. Zudem besteht im Zweifelsfall die Möglichkeit einer bildgebenden – in der Regel CT-gesteuerten – Biopsie bis hin zur Drainage.

**Methode** Durch eine genaue Analyse der Literatur einschließlich der neuesten Artikel werden in dieser Übersicht die grundlegenden und aktuellen bildgebenden Anwendungen für die verschiedenen PPR-Pathologien und das differen-

zialdiagnostische Schema zur Zuordnung der jeweiligen Läsionen exakt beschrieben. Darüber hinaus werden die Einsatzmöglichkeiten der interventionellen Radiologie vorgestellt.

**Ergebnisse** Entsprechend der Häufigkeit werden die verschiedenen Pathologien des PPR von angeborenen Fehlbildungen über Entzündungen bis hin zu Tumoren diskutiert. Charakteristische Kriterien und neuerdings auch der Einsatz fortschrittlicher bildgebender Verfahren und die Einführung der Künstlichen Intelligenz (KI) erlauben eine sehr präzise differenzialdiagnostische Eingrenzung und unterstützen dabei die weitere Diagnostik und Therapie. Nach exakter Zugangsplanung lassen sich nahezu alle Pathologien des PPR mittels CT-gestützter Verfahren biopsieren oder ggf. auch drainieren.

**Schlussfolgerung** Die bildgebende radiologische Diagnostik spielt eine wichtige Rolle bei der Diagnose und Therapieplanung von PPR-Pathologien.

## Kernaussagen

- Läsionen des PPR machen etwa 1–2% aller Pathologien der Kopf- und Halsregion aus. In der Mehrzahl handelt es sich um benigne Läsionen und inflammatorische Prozesse.
- Bleiben differenzialdiagnostische Fragen offen, kann ggf. über eine CT-gesteuerte Biopsie Material gewonnen werden. Ausschlusskriterien sind dabei hypervaskularisierte Prozesse, insbesondere das Paragangliom oder Angiome.
- Der Einsatz Künstlicher Intelligenz (KI) bei der Kopf-Hals-Bildgebung verschiedener Pathologien wie automatische Tumorsegmentierung, pathologische TNM-Klassifikation, Erkennung metastasierter Lymphknoten und extranodale Ausbreitung hat in den letzten Jahren stark zugenommen.

## Introduction

Clinical examination of processes of the parapharyngeal space (PPS) is problematic due to the deep location and the relationship to vessels and nerves. Even large lesions often cannot be detected with examination or palpation.

In contrast, diagnostic imaging uses the complex anatomy of the region for differential diagnosis. The imaging methods primarily used today are contrast-enhanced computed tomography, MRI, and MR angiography and in rare cases also PET-CT. Angiography methods are typically performed for intervention planning or implementation. Current research is focused on the use of artificial intelligence (AI) to diagnose parapharyngeal tumors and determine the prognosis.

The topographic aspects of the PPS, the location with respect to adjacent spaces of the neck, and the options for differential diagnostic classification are presented in the following.

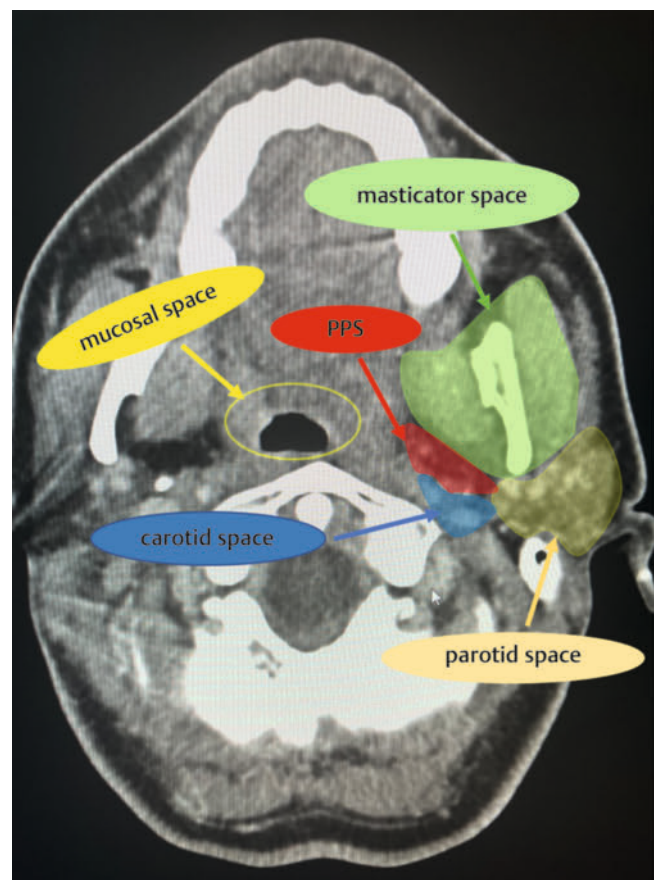
## Anatomy

The PPS is located in the suprahyoid region, is shaped like an upside-down pyramid, and stretches from the base of the skull to the hyoid bone. The PPS is divided into a prestyloid and a poststyloid (carotid space) compartment (by fascia stretching from the styloid to the tensor veli palatini muscle) [1].

### Boundaries of the PPS (► Fig. 1) [2]

- **Medial boundary:** Middle layer of the cervical fascia with the levator veli palatini muscle, the tensor veli palatini muscle, and the constrictor pharyngis superior muscle.
- **Lateral boundary:** Superficial layer of the cervical fascia above the medial wall of the masticator space.
- **Caudal boundary:** The connection between the digastric muscle and the greater horn of the hyoid bone.
- **Superior boundary:** Lower surface of the petrous bone (in the region of the base of the skull).

Precise visualization of the anatomical structure plays an important role in the differentiation of PPS lesions (► Table 1). Moreover, exact knowledge of the particular compartment allows differential diagnosis of lesions located there, primarily masses of the salivary glands, branchiogenic cysts, and lipomas. Lesions in



► Fig. 1 Parapharyngeal space (PPS) and the surrounding deep cervical spaces.

► **Table 1** Contents of the parapharyngeal space.

	Prestyloid compartment	Poststyloid compartment (carotid space)
Contents	Fat	Internal carotid artery
	Small or ectopic salivary gland	Internal jugular vein
	Branch of the mandibular nerve (branch for the tensor veli palatini muscle)	Cranial nerves IX-XII
	Branches of the internal maxillary artery	sympathetic plexus (superior cervical ganglion)
	Ascending pharyngeal artery	Lymph nodes
	Pharyngeal plexus	

the poststyloid compartment are typically paragangliomas, neurogenic tumors, and pathologies involving vessels such as the carotid artery and the jugular vein. Additional parapharyngeal masses can be attributed to metastases, lymph nodes, and other rare tumors.

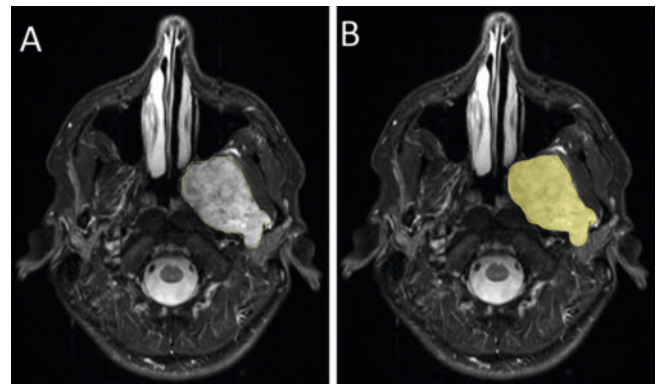
## Imaging methods

Computed tomography (CT) for all pathologies in the head-neck region is usually performed with the use of intravenous contrast agents containing iodine in order to better visualize soft-tissue lesions, inflammatory processes, and adjacent vascular structures. Non-contrast CT can be helpful to determine the presence of calcifications or fat [3]. With the help of dual-energy CT, non-contrast images can be acquired on a secondary basis so that additional use of non-contrast diagnostic imaging is no longer necessary. In the case of highly vascularized masses or compression of vascular structures, CT angiography provides an additional option for reconstruction. These methods are suitable particularly for the evaluation of arterial feeders and venous outflow.

Magnetic resonance imaging (MRI) with its MR angiography techniques is an important examination method for evaluating tumors in the head-neck region due to the excellent soft-tissue visualization without exposure to radiation. The main disadvantage is that image acquisition takes a relatively long time compared to CT and the patient is not allowed to move. In the case of PPS lesions, MRI includes basic sequences (T1w, T2w, T1w+contrast) in addition to fat suppression techniques (TIRM/STIR, Dixon, Spectral Fat sat). Diffusion-weighted imaging is also important for the evaluation of infections and tumors. Vascular and perfusion sequences (e.g., 3D TOF, DCE) are used for vascular malformations and for analyzing tissue perfusion [4].

Nuclear medicine methods: Isotope Imaging can be necessary, e.g., MIBG in paragangliomas, for the diagnosis of some lesions. In the case of suspicion of metastasis or lymphoma, a full diagnostic workup often includes the use of PET-CT.

**Artificial intelligence (AI) and machine learning (ML):** AI allows the use of computer algorithms in order to perform tasks that normally require human intelligence [5]. Machine learning (ML) is a branch of AI that can identify patterns in patient image data with the help of algorithms [6]. Deep learning, a subset of ML, can reduce image noise by using reconstruction methods



► **Fig. 2** **A** and **B** Fat-suppressed T2w MRI showing manual segmentation of a large schwannoma in the parapharyngeal space and left infratemporal fossa of a patient.

applied to raw data and imaging domains. Radiomics: Radiomics refers to the use of quantitative image features to provide prognostic information [6].

The use of AI in head-neck imaging of different pathologies has increased greatly in recent years. Examples of these applications include automatic tumor segmentation (with comparable results to manual segmentation by experts ► **Fig. 2**), pathological TNM classification, tumor staging, differential diagnosis, detection of metastatic lymph nodes, and extranodal metastasis. Moreover, a relatively precise tumor prognosis and treatment response for the particular patient can be determined [6, 7].

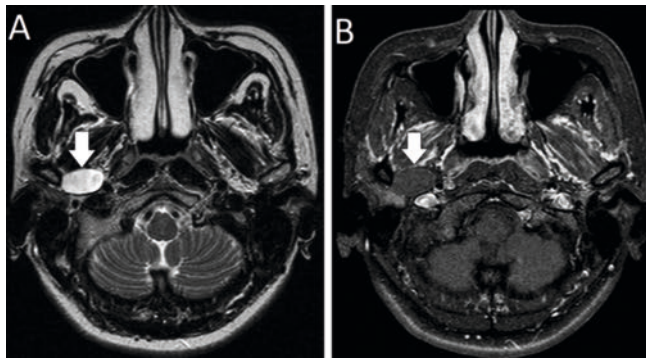
## Imaging criteria: Pathological processes of the PPS

### Congenital malformations

#### Atypical second branchial cleft cyst ► **Fig. 3**

Cysts of the second branchial cleft are the most common anomalies of the branchial cleft. The PPS is a very rare location for a second branchial cleft cyst. These cysts are normally asymptomatic. In rare cases they can cause bulging in the throat or compression of the cranial nerves, particularly in the case of an infection.





► **Fig. 3** **A** Axial MR imaging of a patient with an atypical second branchial cleft cyst, which presents with a hyperintense signal in T2w sequences. **B** There is no contrast enhancement on the post-contrast T1w image.

On CT and MRI, the imaging findings of branchial cleft cysts are similar to those of cysts in other parts of the body. They appear as homogeneous cystic lesions that have clear margins and are filled with fluid (hypodense on CT, low T1 signal and high T2 signal on MRI). Cases with a high protein content can appear relatively hyperdense on CT and have a high T1 signal. Contrast enhancement of the cyst is not seen except in the case of an infection in which case a thin margin of contrast enhancement is possible [8].

### Vascular malformations

Vascular malformations in the PPS are rare. These can occur in the form of venous or lymphatic malformations. Venous malformations (► **Fig. 4**) can resemble a pleomorphic adenoma (which is more common in the PPS). They appear as a well circumscribed mass with mild lobulation and have an isodense signal on CT, an isointense signal on T1w MRI sequences, and a hyperintense signal on T2w MRI sequences. On MRI, signal loss, which can also be confirmed on non-contrast CT, can be present in the case of phleboliths. Contrast enhancement of venous malformations occurs with a delay and washout is slow [9].

Lymphatic malformations usually occur in early childhood. They appear on MRI as multiloculated cystic lesions that occupy multiple spaces of the neck without compressing the surrounding structures [10].

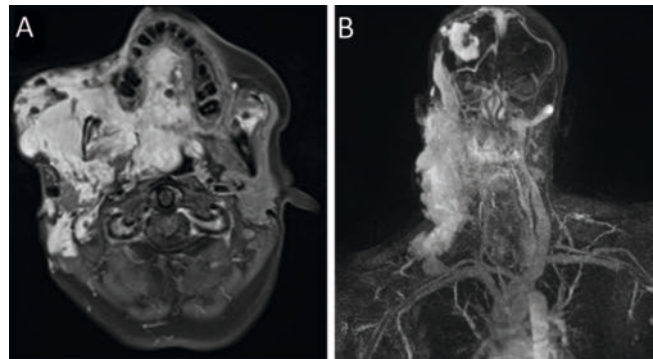
### Inflammation

#### Infection (► **Fig. 5**)

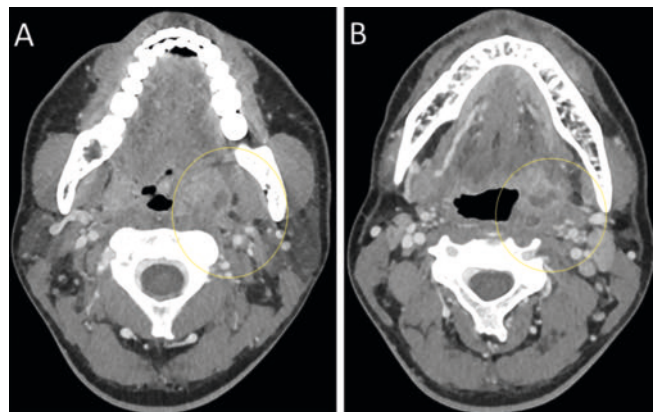
Infections can enter the PPS via the tonsils, teeth, salivary glands, or the middle ear.

A PPS infection appears on CT as edematous thickening of the fat tissue. An increased signal compared to other fat tissues can be seen on T2w MRI and a hyperintense signal on fat-suppressed T1-weighted MRI after contrast administration, indicating abnormal tissue enhancement.

On CT, an abscess appears as a cystic lesion with peripheral enhancement and no enhancement in the center. On MRI, the abscess normally appears to have a center with an abnormal hyperintense T2w signal with a low ADC. Abnormal tissue enhancement sur-

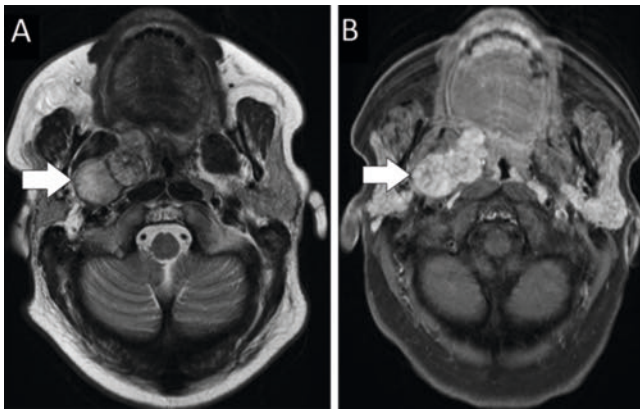


► **Fig. 4** MR imaging of a patient with a giant venous hemangioma. **A** On axial T1w + contrast-enhanced MR imaging, it appears as a soft-tissue mass extending from the frontoparietal region down to the thoracic inlet and occupying several neck spaces including the floor of the mouth, parapharyngeal space, carotid space, masticator space, and parotid space, with additional narrowing of the nasopharynx and oropharynx. **B** MR angiography TWIST-3D MIP image after contrast administration.



► **Fig. 5** **A** Axial CT images of a patient showing a confluent mixed intra-/peritonsillar abscess on the left side with involvement of the parapharyngeal space oropharyngeally and corresponding surrounding perifocal edema/swelling as well as constriction of the air column. **B** In addition, there is an accompanying reactive cervical lymphadenopathy.

rounds this non-enhanced center on T1-weighted images after contrast administration. The main goal of diagnostic imaging is to differentiate between peritonsillar and parapharyngeal abscesses on CT or MRI since this information is essential for treatment selection and for determining the type of surgical procedure. In the case of a peritonsillar abscess, the infection is localized in the mucosal space that is bordered by the middle layer of the cervical fascia. In this case, the fat in the PPS is laterally displaced without the occurrence of an infection. If the infection bypasses the middle layer of the cervical fascia and reaches the PPS, the fat in the PPS is cloudy and causes medial displacement of the tonsils and the pharyngeal mucosa. In both cases, enlarged lymph nodes in the retropharyngeal and the poststyloid compartment of the PPS can be verified. Infections of the poststyloid compartment of the PPS (carotid space) can cause thrombophlebitis of the internal jugular vein. CT images show con-



► **Fig. 6** **A** MRI of a patient with parapharyngeal pleomorphic adenoma on the right. A hyperintense signal is seen on the T2w image. **B** Post-contrast enhancement on T1w + C image.

trast enhancement of the wall of the internal jugular vein and occlusion of the lumen by a thrombus [11].

## Tumors

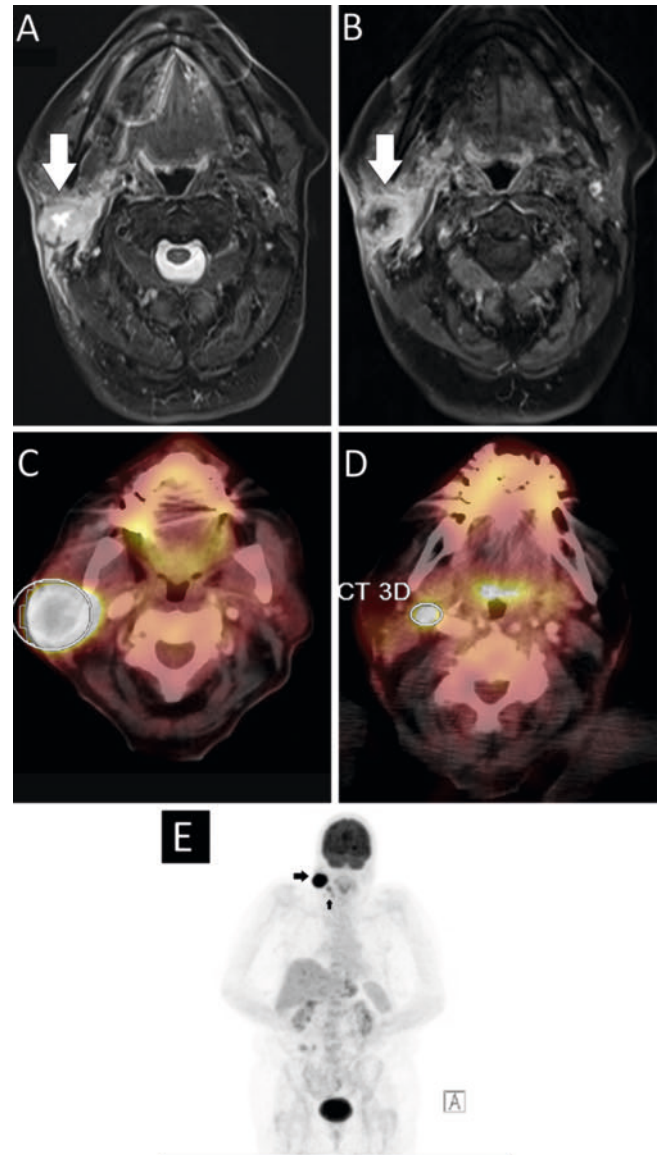
### Salivary gland tumors

The most common tumors in the PPS are salivary gland tumors (40–50%). These are primarily located in the prestyloid PPS. The deep lobe of the parotid gland (no fat layer between the tumor and the parotid gland), ectopic salivary gland tissue, or small salivary glands in the lateral pharyngeal wall (fat layer between the tumor and the parotid gland) are possible origins of these tumors. The most common type of salivary gland tumor is the pleomorphic adenoma (► **Fig. 6**), which comprises 80–90% of all salivary gland neoplasms in the PPS [12]. Pleomorphic adenomas normally appear on CT images as well-defined lesions with smooth margins. They can be inhomogeneous when multiple regions with necrosis or calcifications are included. There is typically strong contrast enhancement. Peripheral contrast enhancement is only seen in a few cases. Pleomorphic adenomas also have a well-defined margin with lobulations on MRI. They appear with an isohypointense signal on T1w images and a significantly hyperintense signal on T2w images (heterogeneous in the case of large lesions). As shown on CT, there is also significant contrast enhancement on MRI. The capsule is typically easier to detect on MRI than on CT images (in the form of a hypointense ring on T2w images) [13]. Other types of benign swelling of the salivary glands can also occur, e.g., Warthin tumor and adenomas.

Malignant salivary gland tumors in the PPS are rare. These include squamous cell carcinoma (► **Fig. 7**), adenoid cystic carcinoma, carcinoma ex pleomorphic adenoma, mucoepidermoid carcinoma, adenocarcinoma, and acinar cell carcinoma [14].

Current studies have shown the potential of deep learning models to differentiate between malignant and benign salivary gland tumors. By using this model, the necessity for a biopsy or surgical resection can be reduced in many patients [15].

Other newer studies have shown the potential for the use of radiomics to differentiate between parapharyngeal pleomorphic



► **Fig. 7** MRI and 18F-FDG PET-CT of a patient with squamous cell carcinoma of the parotid gland. **A** The fat-suppressed T2w sequence shows a round, centrally necrotizing lesion in the caudal pole to the right of the parotid gland extending to the cutis laterally and the parapharyngeal space medially with surrounding edema. **B** The T1w sequence after contrast administration shows strong contrast enhancement. **C** The axial PET-CT fusion image shows increased tracer enhancement in the right parotid mass (SUVmax 24.0). **D** Intense focal enhancement is also documented in the right cervical lymph nodes at level IIa (SUVmax 7.1). **E** Whole-body PET-CT shows focal enhancement in the right parotid lesion and the right cervical lymph nodes.

adenomas and neurogenic tumors based on the texture analysis of T2w images [16].

Deep learning algorithms in combination with an anomaly detection method were also used in a current study to differentiate between benign and malignant salivary gland tumors on MRI [17].

## Neurogenic/vascular tumors

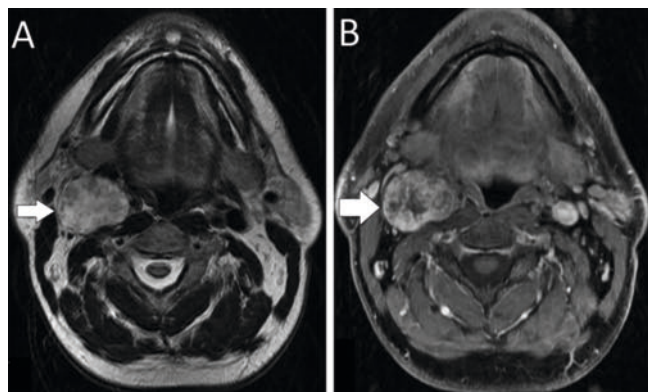
Neurogenic/vascular tumors of the PPS include paragangliomas, neurofibromas, schwannomas, malignant tumors of the peripheral nerve sheath, and malignant paragangliomas [14]. Correct preoperative identification of the nerve origin or peripheral nerve sheath tumors is an important step that can improve surgical results and prognosis. New studies indicate that the carotid-jugular angle can be used for the preoperative prediction of the nerve origin of a tumor. An angle  $\geq 100^\circ$  predicts a vagus origin, while a carotid-jugular angle of  $< 100^\circ$  predicts a non-vagus origin [18].

### Schwannoma (► Fig. 8)

Schwannomas are the most common type of neurogenic tumor in the PPS. The vagus nerve is the most common origin followed by the cervical sympathetic chain [19]. Schwannomas are hypovascularized tumors that do not show increased contrast enhancement in the early contrast phase in dynamic studies. Due to the occlusion of the venous drainage, there is often significant enhancement in the delayed phase of post-contrast sequences. This is an important criterion with respect to hypervascularized tumors like paragangliomas. A heterogeneous hyperintense signal is seen on T2w MRI. Schwannomas appear as well-circumscribed, round to oval, iso-hypodense soft-tissue lesions on CT, usually with moderately heterogeneous contrast enhancement [20]. A recent study tested whether diffusion coefficients (ADC) can be used to differentiate between PPS schwannomas and pleomorphic adenomas on MRI. The results showed that this was possible using the skewness and kurtosis measurements of ADC histograms (high skewness and low kurtosis in schwannomas), although the mean ADC values did not differ [21].

### Paraganglioma (► Fig. 9)

In the case of paragangliomas in the PPS, a primary differentiation should be made between vagal paragangliomas, paragangliomas of the carotid body, glomus jugulare tumors, and tympanic paragangliomas. Combined forms are also possible.

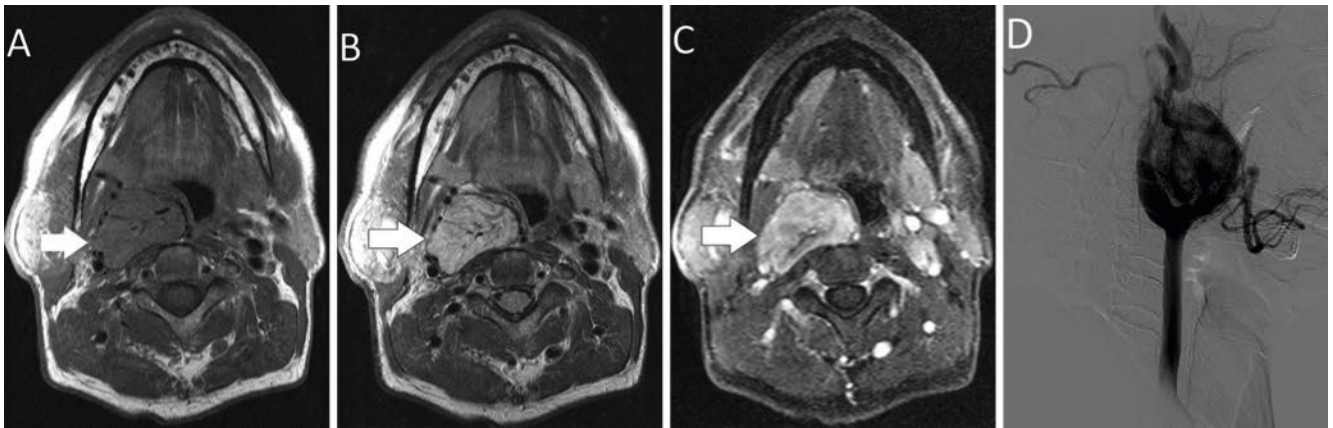


► **Fig. 8** **A** MRI of a patient with a parapharyngeal schwannoma on the right side. A parapharyngeal mass with heterogeneous hyperintense signal in the T2w sequence is documented on the right side. **B** Inhomogeneous contrast enhancement on the T1w + C images.

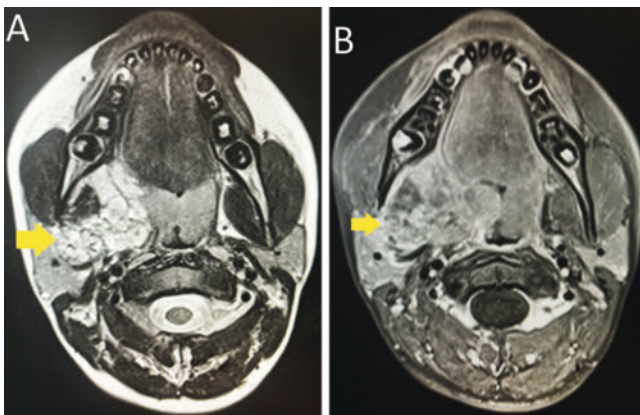
On cross-sectional imaging, paragangliomas typically appear as a well-defined soft-tissue mass at a characteristic location. Tumors of the carotid body occur at the level of the carotid bifurcation causing the external carotid artery and the internal carotid artery to splay. Paragangliomas of the carotid body can be categorized according to the Shamblin classification (for predicting blood loss) depending on the degree of vascular adhesion/vascular contact. (I)  $< 180$  degree contact, (II)  $180\text{--}270$  degree contact, (III)  $> 270$  degree contact. Based on the size and degree of adhesion with the surrounding vessels, the extent to which an operation would be beneficial can be evaluated. Vagal paragangliomas displace the external carotid artery and internal carotid artery anteriorly and the internal jugular vein posteriorly. The Netterville-Glasscock classification divides vagal paragangliomas into three groups: Group A: Confined to the neck, group B: Extending to the jugular foramen, and group C: Invasion of the jugular foramen [22]. Paragangliomas typically have a hypointense signal on T1w MRI images and a moderately hyperintense signal on T2w MRI images. They can be heterogeneous with regions of flow void signals or intralesional bleeding as small hypointense foci on T2w images and small hyperintense foci on T1w images (salt and pepper pattern). Early and strong contrast enhancement is seen on post-contrast MRI [23]. Intralesional vascularization can be further visualized by using non-contrast 3D time of flight (TOF) and a 3D post-contrast sequence. It should be taken into consideration that paragangliomas can occur simultaneously at multiple locations. Therefore, it is always necessary to search for additional paragangliomas [24]. Compared to conventional MRI, advanced MRI techniques can measure the blood flow and evaluate the metabolite composition of paragangliomas. MRI perfusion (MRP) evaluates the blood supply at the level of the capillaries. It can be performed with or without (arterial spin marking) the use of a gadolinium-based contrast agent. MRP hemodynamics show increased blood flow, higher peak enhancement, and a shorter time to peak enhancement in paragangliomas compared to schwannomas. Since paragangliomas have a large capillary network with arteriovenous shunting and a susceptibility to extravascular leaks, they usually have low K<sub>trans</sub> and K<sub>ep</sub> values. MR spectroscopy is not routinely performed in paragangliomas but can yield elevated succinate values (2.4 ppm) in certain cases. Nuclear imaging also plays an important role in paraganglioma imaging. Since, for example, somatostatin analogs like DOTATATE have a significant affinity for certain types of receptors that are overexpressed in extraadrenal paragangliomas, <sup>68</sup>Ga-DOTATATE-PET/CT yielded higher detection of lesions and metastases compared to conventional CT and MRI [21].

In cases with multiple paragangliomas, treatment becomes increasingly challenging due to the complex neurovascular structures that are at risk of being damaged. Preoperative evaluation of the relationship between a tumor and neurovascular structures is thus essential. The introduction of computer-aided 3D models and 3D printed models can be helpful in preoperative planning. Image acquisition for preoperative image and planning data is performed primarily using CT and MRI [25].





► **Fig. 9** **A** MRI of a patient with carotid body. A hypervascular mass is documented in the right parapharyngeal space at the level of the carotid bifurcation in T1w. **B** Flow voids on the unenhanced T2w sequence. **C** Strong inhomogeneous enhancement. **D** Digital subtraction angiography (DSA) showing the highly vascularized tumor in the area of the carotid bifurcation.



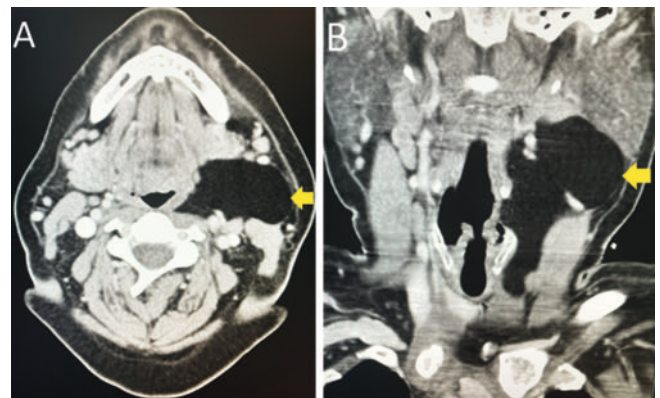
► **Fig. 10** **A** MRI of a patient with neurofibroma in the right parapharyngeal space. It is a heterogeneous T2w image with small cystic areas. **B** Heterogeneous contrast enhancement.

### Neurofibroma (► Fig. 10)

Neurofibromas in the PPS are typically seen in the case of type 1 neurofibromatosis. A solitary neurofibroma is difficult to differentiate from a schwannoma on radiological imaging. Neurofibromas can also occur as multiple hypodense lesions with variations in contrast enhancement and can include multiple deep neck spaces (since they extend along the nerve branches). They appear isointense with respect to muscle on T1w MRI and hyperintense on T2w MRI. Homogeneous/heterogeneous enhancement can also be seen on post-contrast sequences [26].

### Lipoma

Lipomas in the PPS are rare (► Fig. 11). Since lipomas are comprised of fat, they usually have the same signal as subcutaneous fat tissue on CT (non-enhancing lesion with characteristically low density) and MRI (hyperintense on T1w and T2w +/- internal septations). Detection of these lesions is facilitated by the use of lipid suppression sequences on MRI [27].



► **Fig. 11** CT scan of a patient with lipoma in the parapharyngeal space extending caudally along the medial side of the sternocleidomastoid muscle.

### Metastasized adenopathy

Lymph node metastases can also be detected in the PPS. They typically occur in the case of primary tumors from the nasopharynx and oropharynx, rarely also in malignant thyroid tumors.

### Tumors of other spaces of the neck

- A pathology in the surrounding deep neck spaces can result in displacement of the parapharyngeal fat in the prestyloid compartment in various directions. This can help to determine the differential diagnosis for each space. Malignant tumors in adjacent neck spaces can penetrate directly into the PPS.
- The most common pathologies that can occur in the surrounding spaces are shown in ► Table 2.

### Interventional radiology procedures

Invasive angiography or digital subtraction angiography (DSA) (► Fig. 12) is recommended in individual cases for the workup and preinterventional planning for some vascular lesions. This is typically

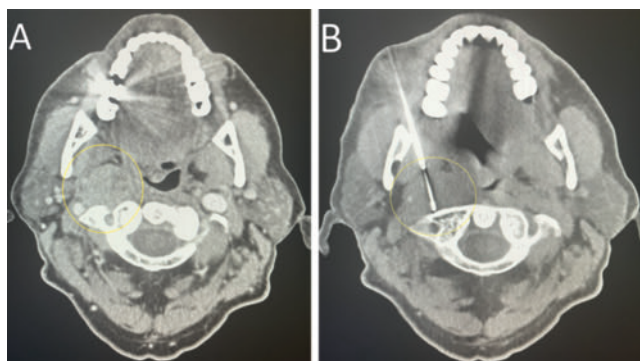
► **Table 2** Compartments in the parapharyngeal space with pathologies.

Compartment	Pathologies
Parotid space	<ul style="list-style-type: none"> <li>Parotid tumors</li> <li>Infections</li> <li>Lymphadenopathies</li> </ul>
Masticator space	<ul style="list-style-type: none"> <li>Odontogenic process</li> <li>Osteomyelitis of the mandible</li> <li>Osteoblastoma</li> <li>Chondrosarcoma</li> <li>Osteosarcoma</li> <li>Hemangioma</li> </ul>
Mucosal space	<ul style="list-style-type: none"> <li>Tonsillitis</li> <li>Tonsillar abscess</li> <li>Tonsillar carcinoma</li> <li>Lymphoma</li> <li>Tumor of the small salivary glands</li> <li>Juvenile nasopharyngeal fibroma</li> </ul>
Retropharyngeal space	<ul style="list-style-type: none"> <li>Reactive adenopathy</li> <li>Cellulitis</li> <li>Abscess</li> <li>Lymph node metastases</li> <li>Lymphoma</li> </ul>
Prevertebral space	<ul style="list-style-type: none"> <li>Metastasis in the region of the spinal column</li> <li>Osteomyelitis with abscess</li> </ul>

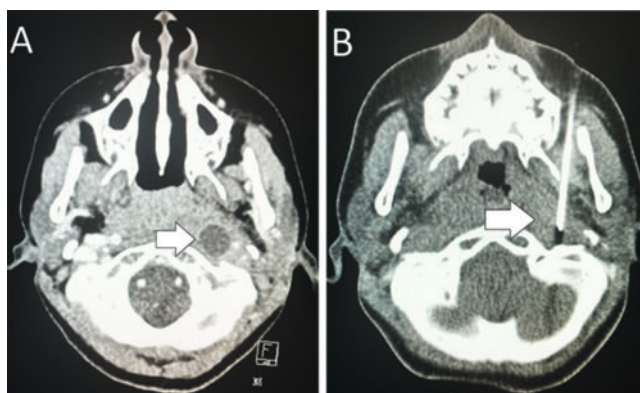


► **Fig. 12** A Digital subtraction angiography (DSA) of the neck vessels in a patient with a parapharyngeal lesion. Selective visualization of the external carotid artery shows multiple feeders with a main feeder from the ascending parapharyngeal artery, but also feeders from the occipital artery supplying the tumor. B The angiography shows significant flushing with an early venous phase. This is most consistent with a glomus tumor.

combined with preoperative embolization therapy and can be planned as a preoperative treatment strategy particularly in the case of paragangliomas, angiofibromas, and intravascular metastases. The goal of tumor embolization is selective occlusion of the external carotid artery or the subclavian artery using various embolization materials. It can be performed immediately before the operation or preoperatively at an interval of 1–3 days to allow occlusion of the necessary vessels without needing to open the collateral circulation. These methods help to reduce blood loss during surgery and to improve the overall prognosis of the patient [28].



► **Fig. 13** A CT-guided puncture of a suspicious parapharyngeal mass for histological confirmation. B After local anesthesia, an 18G puncture cannula was inserted. A careful sample was then taken. No localized complications were noted. The final histological diagnosis was metastatic lymphadenopathy.



► **Fig. 14** A CT scan of a 12-year-old female patient with peritonsillar abscess with left parapharyngeal extension. B CT-guided puncture with complete drainage. After carefully positioning the patient in the supine position (anesthesia) and administering local anesthesia, a puncture needle is inserted into the parapharyngeal space. Aspiration of 3 ml of a bloody, creamy, purulent fluid. Complete evacuation is achieved by removing the hypodense margin.

Newer strategies allow primary use of embolization techniques also in the case of complex infiltrative paragangliomas and vascular metastases for downsizing and for location control of inoperable tumors.

**CT-guided biopsy** (► **Fig. 13**) – CT is the method of choice for image-guided biopsies of deep PPS lesions that cannot be reached clinically. In some cases, MRI or ultrasound can also be used. This is usually performed using non-contrast CT. However, in the case of lesions in close connection to the carotid artery, a contrast agent can be used. In many cases, the operation is performed under local anesthesia or sedation. However, general anesthesia is also possible in some cases. Neck biopsies in the suprahyoid region can be performed using various access routes, e.g., subzygomatic, retromandibular, paramaxillary, submastoid, and transoral. These interventions are typically performed without major complications (e.g. damage to important blood vessels and nerves) when well-planned and performed by an expert. However, minor



complications like pain, mild infections, bleeding, and/or vasovagal reactions can occur [28].

**CT-guided drainage** (► **Fig. 14**) – As in CT-guided biopsies, abscesses and large cysts are drained and drainage tubes are placed under CT guidance.

**Other radiological interventions** can also be used, in particular percutaneous sclerotherapy in venous and lymphatic malformations, intraarterial chemotherapy in carcinomas, and intraarterial chemotherapy as well as embolization in symptomatic tumors or lymph node metastases.

## Conflict of Interest

The authors declare that they have no conflict of interest.

## References

- [1] Bulut OC, Giger R, Alwagdani A et al. Primary neoplasms of the parapharyngeal space: diagnostic and therapeutic pearls and pitfalls. *Eur Arch Otorhinolaryngol* 2021; 278 (12): 4933–4941. doi:10.1007/s00405-021-06718-4
- [2] Koenig LJ, Tamimi D, Perschbacher SE. Parapharyngeal space. In: Koenig LJ, Tamimi D, Perschbacher SE, Eds.; *Diagnostic Imaging part I: Oral and Maxillofacial* second ed. Elsevier; 2017: 168–171
- [3] Dammann F, Bootz F, Cohnen M et al. Diagnostic imaging modalities in head and neck disease. *Dtsch Arztebl Int* 2014; 111: 417–423. doi:10.3238/arztebl.2014.0417
- [4] Widmann G, Henninger B, Kremser C et al. MRI Sequences in Head & Neck Radiology – State of the Art. *MRI-Sequenzen in der Kopf-Hals-Radiologie – State of the Art. Fortschr Röntgenstr* 2017; 189 (5): 413–422. doi:10.1055/s-0043-103280
- [5] Pham N, Ju C, Kong T et al. Artificial Intelligence in Head and Neck Imaging. *Semin Ultrasound CT MR* 2022; 43 (2): 170–175. doi:10.1053/j.sult.2022.02.006
- [6] Chinnery T, Arifin A, Tay KY et al. Utilizing Artificial Intelligence for Head and Neck Cancer Outcomes Prediction From Imaging. *Canadian Association of Radiologists Journal* 2021; 72 (1): 73–85. doi:10.1177/0846537120942134
- [7] Tortora M, Gemini L, Scaravilli A et al. Radiomics Applications in Head and Neck Tumor Imaging: A Narrative Review. *Cancers (Basel)* 2023; 15 (4): 1174. doi:10.3390/cancers15041174.
- [8] Shin JH, Lee HK, Kim SY et al. Parapharyngeal second branchial cyst manifesting as cranial nerve palsies: MR findings. *AJNR Am J Neuroradiol* 2001; 22 (3): 510–512
- [9] Tomblinson CM, Fletcher GP, Lidner TK et al. Parapharyngeal Space Venous Malformation: An Imaging Mimic of Pleomorphic Adenoma. *AJNR Am J Neuroradiol* 2019; 40 (1): 150–153. doi:10.3174/ajnr.A5859
- [10] Shin JH, Lee HK, Kim SY et al. Imaging of parapharyngeal space lesions: focus on the prestyloid compartment. *AJR Am J Roentgenol* 2001; 177 (6): 1465–1470. doi:10.2214/ajr.177.6.1771465
- [11] Hirvonen J, Heikkinen J, Nyman M et al. MRI of acute neck infections: evidence summary and pictorial review. *Insights Imaging* 2023; 14 (1): 5. doi:10.1186/s13244-022-01347-9.
- [12] Akin I, Karagöz T, Mutlu M et al. Pleomorphic adenomas of the parapharyngeal space. *Case Rep Otolaryngol* 2014; 2014: 168401. doi:10.1155/2014/168401
- [13] Kakimoto N, Gamoh S, Tamaki J et al. CT and MR images of pleomorphic adenoma in major and minor salivary glands. *Eur J Radiol* 2009; 69 (3): 464–472. doi:10.1016/j.ejrad.2007.11.021
- [14] Riffat F, Dwivedi RC, Palme C et al. A systematic review of 1143 parapharyngeal space tumors reported over 20 years. *Oral Oncol* 2014; 50 (5): 421–430. doi:10.1016/j.oraloncology.2014.02.007
- [15] Xia X, Feng B, Wang J et al. Deep Learning for Differentiating Benign From Malignant Parotid Lesions on MR Images. *Front Oncol* 2021; 11: 632104. Published 2021. doi:10.3389/fonc.2021.632104
- [16] Zheng X, Huang C, Yu B et al. Differentiation of neurogenic tumours and pleomorphic adenomas in the parapharyngeal space based on texture analysis of T2WI. *BMC Oral Health* 2023; 23(1): 548. Published 2023. doi:10.1186/s12903-023-03283-6
- [17] Faur AC, Buzaş R, Lăzărescu AE et al. Current Developments in Diagnosis of Salivary Gland Tumors: From Structure to Artificial Intelligence. *Life* 2024; 14 (6): 727. doi:10.3390/life14060727
- [18] Wong CE, Huang CC, Chuang MT et al. Quantification of vessel separation using the carotid-jugular angle to predict the nerve origin of neck peripheral nerve sheath tumours: a pooled analysis of cases from the literature and a single-center cohort. *Int J Surg* 2023; 109(9): 2704–2713. Published 2023. doi:10.1097/J9.0000000000000491
- [19] Katre MI, Telang RA. Schwannoma of parapharyngeal space: a case report. *Indian J Surg* 2015; 77 (1): 79–81. doi:10.1007/s12262-013-0911-7
- [20] Kulkarni M. Vagal Schwannoma and Carotid Body Tumor: Magnetic Resonance Imaging Appearance and Differential Diagnosis. *Int J Head Neck Surg* 2015; 6 (4): 195–196
- [21] Kunimatsu N, Kunimatsu A, Miura K et al. Differentiation between pleomorphic adenoma and schwannoma in the parapharyngeal space: histogram analysis of apparent diffusion coefficient. *Dentomaxillofacial Radiology* 2023; 52 (7): 20230140. doi:10.1259/dmfr.20230140
- [22] Lin EP, Chin BB, Fishbein L et al. Head and Neck Paragangliomas: An Update on the Molecular Classification, State-of-the-Art Imaging, and Management Recommendations. *Radiol Imaging Cancer* 2022; 4 (3): e210088. doi:10.1148/rycan.210088
- [23] McClelland AC, Shifteh K, Burns J. Advances in Head and Neck Paraganglioma Imaging. *Adv Clin Radiol* 2022; 4 (1): 195–214
- [24] Heckl S, Bösmüller H, Ioanoviciu SD et al. Imaging Diagnosis of Glomus Tumors of the Head and Neck – Bildgebung bei Glomustumoren des Kopfes und Halses (Paragangliom, Chemodektoma). *Fortsch Röntgenstr* 2015; 187 (6): 409–414. doi:10.1055/s-0035-1552000
- [25] Li L, Xu H, Chen X et al. Management of Multiple Head and Neck Paragangliomas With Assistance of a 3-D Model. *Ear, Nose & Throat Journal* 2023; 102 (6): 362–368. doi:10.1177/01455613211009441
- [26] Mukherji SK, Chong V. Neurofibroma. In: Mukherji SK, Chong V, Eds.; *Atlas of Head and Neck Imaging* Stuttgart: Thieme; 2004
- [27] Pal P, Singh B, Sood AS. Unusual parapharyngeal lipoma. *Indian J Otolaryngol Head Neck Surg* 2015; 67 (Suppl. 1): 158–160. doi:10.1007/s12070-014-0797-0.
- [28] Gandhi D, Gemmete JJ, Ansari SA et al. Interventional neuroradiology of the head and neck. *AJNR Am J Neuroradiol* 2008; 29 (10): 1806–1815. doi:10.3174/ajnr.A1211